Helical Junctions as Determinants for RNA Folding: Origin of Tertiary Structure Stability of the Hairpin Ribozyme†

Dagmar Klostermeier and David P. Millar*

Department of Molecular Biology, The Scripps Research Institute, MB-19, 10550 North Torrey Pines Road, La Jolla, California 92037

Received June 20, 2000; Revised Manuscript Received August 25, 2000

ABSTRACT: Helical junctions are ubiquitous structural elements that govern the folding and tertiary structure of RNAs. The tobacco ringspot virus hairpin ribozyme consists of two helix−loop−helix elements that lie on adjacent arms of a four-way junction. In the active form of the hairpin ribozyme, the loops are in proximity. The nature of the helical junction determines the stability of the hairpin ribozyme tertiary structure [Walter, N. G., Burke, J. M., and Millar, D. P. (1999) *Nat. Struct. Biol. 6*, 544−549] and thus its catalytic activity. We used two-, three-, and four-way junction hairpin ribozymes as model systems to investigate the thermodynamic basis for the different tertiary structure stabilities. The equilibrium between docked and extended conformers was analyzed as a function of temperature using time-resolved fluorescence resonance energy transfer (trFRET). As the secondary and tertiary structure transitions overlap, information from UV melting curves and trFRET had to be combined to gain insight into the thermodynamics of both structural transitions. It turned out that the higher tertiary structure stability observed in the context of a four-way junction is the result of a lower entropic cost for the docking process. In the two- and three-way junction ribozymes, a high entropic cost counteracts the favorable enthalpic term, rendering the docked conformer only marginally stable. Thus, two- and three-way junction tertiary structures are more sensitive toward regulation by ligands, whereas four-way junctions provide a stable scaffold. Altogether, RNA folding and stability appear to be governed by principles similar to those for the folding of proteins.

Proteins as well as nucleic acids have to form defined three-dimensional structures as a prerequisite for their biological functions. Whereas numerous studies have revealed pathways of protein folding, the principles of RNA folding are only beginning to emerge. Recent studies corroborated the expectation that RNA folding pathways are complex and are governed by a rugged energy landscape (*2*−*5*).

Helical junctions are ubiquitous elements of RNA structures. The local structure of a junction determines the overall arrangement of helices within the folded structure of RNA molecules. In addition, conformational changes of junctions can induce large rearrangements in distant regions of an RNA molecule. Therefore, helical junctions are considered to be important determinants for RNA structure formation as well as crucial regulatory elements.

Ribozymes have been extensively used to study structure−function relationships in RNA as their catalytic activity directly reports on the correct structure being formed. The hairpin ribozyme from tobacco ringspot virus satellite RNA has proven to be a convenient model system for studying the influence of substructures on folding. A minimal hairpin ribozyme comprises two helix−loop−helix elements, with the catalytically important nucleotides being located in the loops (*6*−*8*). The loop regions have to come into proximity to allow for tertiary interactions that stabilize the active, docked conformer (*1*, *9*−*13*). In tobacco ringspot virus, these two loops are located on two arms of a four-way junction (4WJ)[1] (*14*). Variants of the hairpin ribozyme containing a two-way or three-way helical junction (2WJ or 3WJ, respectively) have also been investigated. The nature of the helical junction was shown to determine the stability of the docked hairpin ribozyme (*1*). In the context of a 4WJ, the active docked conformation is highly favored (95%) whereas ribozymes containing a 2WJ or 3WJ exist in the inactive extended conformer to a significant extent (35 or 60%, respectively). Thus, the hairpin ribozyme seems to be optimized with the 4WJ as a scaffold to favor specific interactions between distant domains.

In thermodynamic terms, both enthalpic or entropic contributions may account for the enhanced stabilization of the docked conformer in the context of a 4WJ. It can be envisaged that additional tertiary interactions are formed with a 4WJ. Alternatively, the entropy change during docking may be less unfavorable in the context of a 4WJ. The enthalpic and entropic contributions to tertiary structure stability can be quantified from the temperature dependence of the docking equilibrium. This information can be gained from time-resolved fluorescence resonance energy transfer (trFRET) experiments performed at different temperatures with ribozymes that are labeled with fluorescein (donor) and

† This work was supported by NIH Grant GM 58873 (to D.P.M.) and an EMBO fellowship (to D.K.).

* Corresponding author. Phone: (858) 784-9870. Fax: (858) 784-9067. E-mail: millar@scripps.edu.

[1] Abbreviations: 2WJ, 3WJ, and 4WJ, two-way, three-way, and four-way helical junction, respectively; trFRET, time-resolved fluorescence resonance energy transfer.

10.1021/bi0014103 CCC: $19.00
Published on Web 09/29/2000

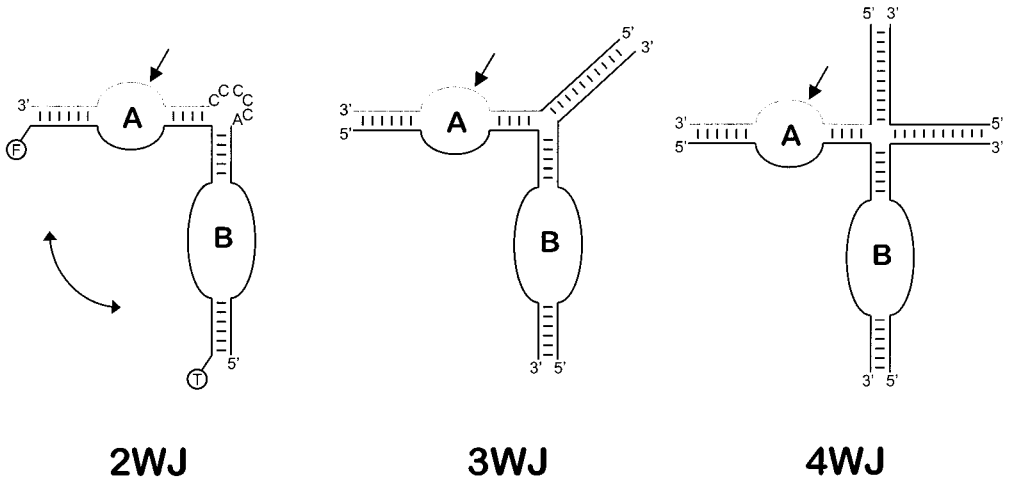

FIGURE 1: Schematic representation of the 2WJ, 3WJ, and 4WJ hairpin ribozymes. Loop A and loop B carry the essential nucleotides for endonuclease activity. The arrow denotes the potential cleavage site in loop A. In this study, hairpin ribozymes with a 2′-deoxy modification at this position were used to avoid cleavage. The donor fluorophore fluorescein (F) and the acceptor fluorophore tetramethylrhodamine (T) are attached to the ends of the two helical arms carrying the loops as indicated for the 2WJ. In the docked ribozyme, the two loops approach each other, indicated by the double-headed arrow, resulting in a decreased donor−acceptor distance and a higher FRET efficiency.

tetramethylrhodamine (acceptor) on the helical arms carrying the loops (Figure 1). trFRET measures the influence of an acceptor fluorophore on the fluorescence decay of the donor. The decays can be analyzed in terms of continuous Gaussian distributions of the interfluorophore distance, allowing for resolution of two or more conformers in equilibrium. The resulting fractional populations define the equilibrium constant and the corresponding free energy difference.

We used the hairpin ribozyme as a model system to investigate the thermodynamic basis of RNA tertiary structure formation in 2WJ, 3WJ, and 4WJ ribozymes (Figure 1). Thermal undocking profiles obtained for each ribozyme by trFRET were compared to quantify the effect of junction structure on overall stability. As undocking is coupled to overall dissociation of the complex at elevated temperatures, a trFRET analysis was employed which includes information from UV melting curves. With this method, tertiary structure conformers can be reliably quantified across a range of temperatures, even with the background of overlapping secondary structure transitions. Surprisingly, the enhancement of tertiary structure stability by a 4WJ was found to be entirely entropic in origin. The 4WJ reduced the entropic cost of docking compared with 2WJ and 3WJ ribozymes, suggesting that the 4WJ stabilizes docking by restricting the conformational freedom of the undocked complex. The implications of these findings for the effect of helical junctions on conformational changes and formation of RNA structure are discussed.

EXPERIMENTAL PROCEDURES

Preparation of RNA Samples. RNA strands were synthesized, labeled, and purified as described previously (*1*). The sequences were 5′-fluorescein-AAA UAG AGA AGC GAA CCA GAG AAA CAC ACG CC-tetramethylrhodamine-3′ and 5′-GGC GUG GUA CAU UAC CUG GUA CCC CCU CGC dAGU CCU AUU U-3′ (2WJ), 5′-GGC GUG GUA CAU UAC CUG GUA CGA GUU GAC-3′ and 5′-GUC AAC UCG UUC GCdA GUC CUA UUU-3′ (3WJ), or 5′-GGC GUG GUA CAU UAC CUG GUA CGA GUU GAC-3′, 5′-GUC AAC UCG UGG UGG CUU GC-3′, and 5′-GCA AGC CAC CUC GCdA GUC CUA UUU-3′ (4WJ).

RNA complexes were prepared in 50 mM Tris-HCl (pH 7.5) and 1 mM $MgCl_2$ at a labeled strand concentration of 1 μM and a 3-fold molar excess of the unlabeled strand(s). The strands were annealed by heating to 70 °C for 2 min and cooling to ambient temperature within 5 min.

UV Melting Curves. UV melting curves were recorded on a AVIV 14DS UV−vis spectrophotometer in 300 μL cuvettes. The annealed sample was heated at a rate of 0.5 °C/min, and the hyperchromicity was followed at 260 nm. Absorbance spectra were recorded before and after melting and after cooling to the starting temperature to verify the reversibility of the transitions. The contribution of the excess of unlabeled strands to the melting profiles was corrected by subtracting a scan with these strands alone (2 μM concentration), measured under identical conditions.

Melting profiles were analyzed using the program Scientist (Micromath). K'_{anneal} was defined according to eq 1:

$$K'_{\text{anneal}} = \frac{\text{native}}{\text{unfolded}} = \frac{\text{docked} + \text{extended}}{\text{unfolded}} \qquad (1)$$

The primes indicate the apparent thermodynamic values derived from this definition. A linear dependence of the absorbance of both the native (both the docked and extended conformer) and unfolded species on temperature was assumed. Nonlinear least-squares fitting according to eq 2 yields the $\Delta H^{\circ\prime}_{\text{anneal}}$ and the midpoint of the melting transition, T_M.

$$K'_{\text{anneal}} = \exp\left[\frac{\Delta \text{H}^{\circ\prime}_{\text{anneal}}}{R}\left(\frac{1}{T_M} - \frac{1}{T}\right)\right] \qquad (2)$$

$\Delta S^{\circ\prime}_{\text{anneal}}$ and $\Delta G^{\circ\prime}_{\text{anneal}}$ were calculated according to eqs 3 and 4, assuming $K'_{\text{anneal}} = 1$ when $T = T_m$:

$$\Delta S^{\circ\prime}_{\text{anneal}} = \frac{\Delta H_{\text{anneal}}{}^{\circ\prime}}{T_M} \qquad (3)$$

$$\Delta G^{\circ\prime}_{\text{anneal}} = \Delta H_{\text{anneal}}{}^{\circ\prime} - T\Delta S^{\circ\prime}_{\text{anneal}} \qquad (4)$$

The fraction of single-stranded (unfolded) RNA at each temperature was calculated during the fit and was entered

as a fixed parameter into the distance distribution analysis (see below).

Fluorescence Measurements and Decay Analysis. Time-resolved emission profiles were collected using time-correlated single-photon counting as described previously (*15*). Pulsed excitation was achieved with a mode-locked argon ion laser at 514 nm, and the emission was detected at 530 nm (16 nm slit width and 530 nm cutoff filter) under magic angle conditions. The decays were collected in 4096 channels with a time increment of 10 ps per channel. Forty thousand counts were accumulated in the peak of the decay curve. Samples were equilibrated at the respective temperature for 15 min prior to the measurement. To avoid evaporation at elevated temperatures, the solution was covered with PCR oil (light mineral oil, Fisher). Control experiments were performed to ensure that the oil layer does not affect fluorescence lifetimes.

At each temperature, the fluorescence decays of the RNA complex containing only fluorescein and containing both fluorescein (donor) and tetramethylrhodamine (acceptor) were collected. Additionally, the decays of the singly and doubly labeled strand common to all three junctions (see Experimental Procedures) were recorded. A sum-of-exponentials fit to the donor-only decays (eq 5) yielded the intrinsic lifetimes τ_i and amplitudes α_i.

$$I_D = \sum_i \alpha_i \exp\left(-\frac{t}{\tau_i}\right) \quad (5)$$

The decays of the doubly labeled samples were analyzed according to eqs 6 and 7

$$I_{DA} = \sum_k f_k \int P_k(R) \sum_i \alpha_i \exp\left[-\frac{t}{\tau_i}\left(1 + \frac{R_0^6}{R^6}\right)\right] dR \quad (6)$$

$$P_k(R) = 4\pi R^2 c_k \exp[-a_k(R - b_k)^2] \quad (7)$$

Equation 6 incorporates one or more distinct donor−acceptor species, each with a fractional population f_k and a distribution function $P_k(R)$ describing the donor−acceptor distance. Each distribution is described by the shape parameters a_k and b_k and the normalizing factor c_k. The critical transfer distance, R_0, for the fluorescein−tetramethylrhodamine donor−acceptor pair has been determined to be 55 Å (*1*).

Evaluation of the corresponding decay data for the doubly labeled strand alone allowed for determination of the temperature dependence of the donor−acceptor distance after dissociation of the ribozyme strands. In fitting decays for the ribozyme complexes, the fraction of single-stranded RNA as obtained from the UV melting profile analysis at the respective temperature, and the parameters describing the distance distribution for this species were kept constant during the fits. Adjustable parameters were the fractions of the docked and undocked state and their distance distribution. The sum of all fractions was restrained to be equal to unity (eq 8):

$$\text{fraction docked} + \text{fraction extended} + \text{fraction single strand} = 1 \quad (8)$$

van't Hoff Analysis. The equilibrium constant for docking, K_{dock}, was calculated from the fitted fractions of docked and extended conformers (eq 9):

$$K_{dock} = \frac{\text{fraction docked}}{\text{fraction extended}} \quad (9)$$

Likewise, K_{anneal} was calculated from the fractions of extended conformer and single strand (eq 10):

$$K_{anneal} = \frac{\text{fraction extended}}{\text{fraction single strand}} \quad (10)$$

This definition of K_{anneal} is different from the apparent equilibrium constant K'_{anneal} in the analysis of the UV melting curves, where the sum of the fractions of docked and extended ribozymes appeared in the numerator (eq 1).

van't Hoff plots for annealing[2] (secondary structure formation) were analyzed using eq 11 with $\Delta H°_{anneal}$ and $\Delta S°_{anneal}$ as adjustable parameters.

$$\ln K_{anneal} = -\frac{\Delta H_{anneal}°}{RT} + \frac{\Delta S_{anneal}°}{R} \quad (11)$$

van't Hoff plots for docking (tertiary structure formation) were fitted with a generalized form of eq 11 that allows for changes in heat capacity (eq 12).

$$\ln K_{dock} = \frac{\Delta C_p°}{R}\left(\frac{T_H}{T} - \ln\frac{T_S}{T} - 1\right) \quad (12)$$

where T_H and T_S are the characteristic temperatures at which $\Delta H°$ and $\Delta S°$ become zero, respectively. The change in heat capacity, $\Delta C_p°$, and the characteristic temperatures, T_H and T_S, were used as fitting parameters. With the resulting values obtained from the fit, $\Delta H°_{dock}$ and $\Delta S°_{dock}$ at any given temperature can be calculated according to eqs 13 and 14

$$\Delta H_{dock}° = \Delta C_p°(T - T_H) \quad (13)$$

$$\Delta S_{dock}° = \Delta C_p° \ln\left(\frac{T}{T_S}\right) \quad (14)$$

Global Fits for Obtaining Thermodynamic Data on Docking and Annealing. Equations 11 and 12 were used to fit simultaneously the thermodynamic parameters for docking and annealing to the temperature dependence of the fractional populations of docked, undocked, and single-strand species with the program Scientist (Micromath). The global analysis was based on a model assuming two consecutive transitions, a tertiary structure transition (undocking) that is accompanied by a change in heat capacity (eq 11) and a subsequent secondary structure transition (dissociation) with $\Delta H°$ and $\Delta S°$ being independent of temperature (eq 12). The program calculated the fractions of docked, extended, and dissociated species at each temperature on the basis of the values of $\Delta C_p°$, T_H, and T_S (tertiary structure formation) and $\Delta H°_{anneal}$ and $\Delta S°_{anneal}$ (secondary structure formation). The values of these parameters were iterated to obtain the best global fit to the experimental data.

Error propagation for $\Delta H°_{dock}$ and $\Delta S°_{dock}$ derived from the fitting results for $\Delta C_p°$, T_H, and T_S was calculated

[2] For purposes of clarity, throughout the manuscript the term "annealing" has been used to describe formation of secondary structure while the term "docking" refers to tertiary structure formation.

according to the Gaussian rule (eq 15):

$$f = \sqrt{\left(\frac{\partial F}{\partial x_1}\right)^2 s_{x_1}{}^2 + \left(\frac{\partial F}{\partial x_2}\right)^2 s_{x_2}{}^2 + ...} \qquad (15)$$

where f is the standard deviation for the calculated parameter F, which depends on the fitting results x_1, x_2, ..., and s_{x_1}, s_{x_2}, ..., denote the standard deviations for the parameters x_1, x_2, ..., respectively, as calculated by the Scientist program.

RESULTS

Previous studies on hairpin ribozyme docking performed with 12 mM $MgCl_2$ have shown that the tertiary structure of the 2WJ and 3WJ ribozymes can be disrupted by raising the temperature to around 40 °C. The 4WJ ribozyme, however, remains stably docked under these conditions even at 60 °C (*1*). With the Mg^{2+} concentration lowered to 1 mM, which represents physiological conditions, undocking experiments with all three junctions under the same conditions became possible within the spectroscopically accessible temperature range between 4 and 75 °C.

UV Melting Profiles. To define a temperature range in which undocking can be monitored without interference of secondary structure transitions, UV melting profiles of the 2WJ, 3WJ, and 4WJ ribozymes (Figure 1) were recorded under the same conditions that were used in trFRET experiments (1 μM labeled strand and 3 μM unlabeled strands). The contributions of the strands in excess to the A_{260} were measured in a control experiment (2 μM nonlabeled strands) and subtracted from the original profiles. This procedure was necessary to ensure that the thermodynamic data derived from the melting curves describe quantitatively the conditions in the trFRET experiments. In addition, the UV melting curves of an intact 4WJ and a 4WJ $G_{+1}A$ mutant impaired in docking were recorded (data not shown) to test if the ribozyme tertiary structure transition contributes to the change in A_{260}. The two profiles overlay, which confirms that undocking is not accompanied by an increase in A_{260}, and the UV absorbance is only sensitive to changes in secondary structure.

Figure 2 shows the melting curves of the 2WJ, 3WJ, and 4WJ ribozymes and the fits obtained using a two-state model. The midpoints of the secondary structure transitions are at 48 (2WJ), 50 (3WJ), and 68 °C (4WJ). All three junctions show a single transition, suggesting simultaneous, cooperative disruption of all helical structures. Table 1 summarizes the thermodynamic parameters for annealing of the ribozyme complexes. As expected from the different numbers of base pairs formed in each complex, the 2WJ is slightly less stable than the 3WJ, and both are significantly less stable than the 4WJ. Likewise, the favorable enthalpic term is similar for the 2WJ and 3WJ ribozymes (−149 and −188 kJ/mol, respectively), whereas it is twice as high for the 4WJ complex (−372 kJ/mol). All junctions exhibit strong enthalpy−entropy compensation, however, with the lowest entropic cost for secondary structure formation in the 2WJ (−462 J mol^{-1} K^{-1}) and the highest in the 4WJ (−1091 J mol^{-1} K^{-1}). The compensation is most pronounced for the 2WJ and 3WJ ribozymes, leaving a small stabilization energy of −10.7 and −14.7 kJ/mol, respectively, whereas the 4WJ secondary structure is stabilized by −46.9 kJ/mol.

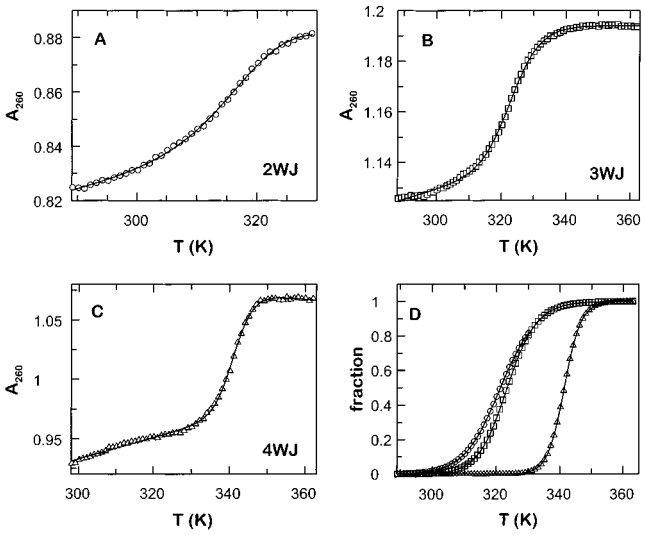

FIGURE 2: UV melting curves of the 2WJ, 3WJ, and 4WJ ribozymes: (A) 2WJ, (B) 3WJ, and (C) 4WJ. The melting profiles were recorded at a heating rate of 0.5 °C/min in 50 mM Tris-HCl (pH 7.5) and 1 mM $MgCl_2$. The fit obtained on the assumption of a two-state model (—) yields $\Delta H°'_{anneal}$ values of −149 (2WJ), −188 (3WJ), and −372 kJ/mol (4WJ). The T_m values are 321 (48 °C), 323 (50 °C), and 341 K (68 °C), respectively. Panel D shows the fraction of dissociated ribozyme calculated from the fit: 2WJ (○), 3WJ (□), and 4WJ (△).

Table 1: Thermodynamics of Ribozyme Secondary Structure As Determined from UV Melting Curves[a]

	2WJ	3WJ	4WJ
$\Delta H°'_{anneal}$ (kJ/mol)	−149 (±14)	−188 (±4)	−372 (±11)
T_m (K)	321 (±2)	323.5 (±0.1)	341.3 (±0.1)
$\Delta S°'_{anneal}$ (J mol^{-1} K^{-1})	−462 (±44)	−582 (±12)	−1091 (±32)
$\Delta G°'_{anneal}$ (kJ mol^{-1})	−10.7	−14.7	−46.9

[a] The data were evaluated according to a two-state model. From $\Delta H°'_{anneal}$ and T_m and their standard deviations, $\Delta S°'_{anneal}$ and $\Delta G°'_{anneal}$ at 25 °C were calculated as described in Experimental Procedures. The prime indicates the apparent thermodynamic values based on the definition of K'_{anneal} in eq 1.

The fraction of dissociated complexes can be calculated at each temperature from the UV melting data (Figure 2D). The 2WJ secondary structure begins to melt above 30 °C, while the 3WJ and 4WJ ribozymes start melting above 40 and 60 °C, respectively. A comparison with preliminary trFRET measurements revealed, however, that melting of ribozyme secondary structure overlaps with the tertiary structure transition (undocking). Thus, it was not possible to confine the trFRET measurements on tertiary structure disruption to a temperature range where the secondary structure is maintained. Instead, dissociated ribozyme complexes had to be taken into account as a third species in addition to docked and undocked ribozymes in the analysis of the trFRET data.

trFRET Experiments. trFRET has been shown to be a sensitive probe that reports on tertiary structure formation of a ribozyme labeled with fluorescein (donor) and tetramethylrhodamine (acceptor) on opposite ends of the two helix−loop−helix segments (*1*). When the loops are docked, the donor−acceptor distance is reduced, resulting in an increased efficiency of energy transfer and a concomitant decrease in donor fluorescence lifetimes. The donor−acceptor distance in the undocked (inactive) hairpin ribozyme is ∼75 Å, and decreases to ∼36 Å in the docked conformer.

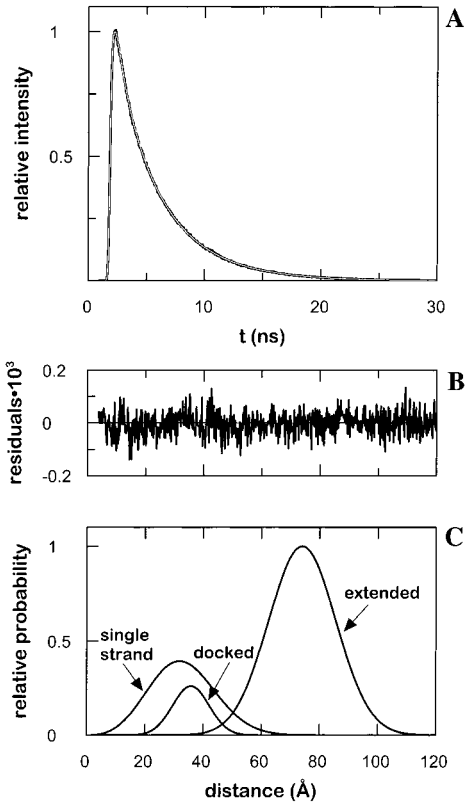

FIGURE 3: Distance fit of the donor decay in the presence of the acceptor with three species. (A) Donor fluorescence decay of a doubly labeled 3WJ ribozyme at 45 °C and fit to a three-species distance distribution (gray line). (B) Weighted residuals of the fit. (C) Distance distribution for the docked, extended, and dissociated ribozyme (centered around 36, 74, and 33 Å, respectively). The distance distribution for the dissociated ribozyme was determined in separate experiments on the labeled single strand alone and was kept fixed in the fit shown here. The fractional population of the dissociated ribozyme was calculated from the UV melting data and kept constant as well. The χ^2 value of the fit is 1.08.

At elevated temperatures, the single strand carrying the fluorophores that is released upon dissociation of ribozyme complexes also contributes to the FRET signal, as the distance between fluorescein and tetramethylrhodamine attached to both ends is similar to the value for the docked conformer. This observation suggests that the single strand is not extended but rather forms a coiled structure similar to the random coil of unfolded proteins.

Consequently, the fluorescence decays have to be analyzed in terms of three species, each with characteristic Gaussian distance distributions, at temperatures where UV melting curves indicate a significant population of the dissociated state. To reduce the number of free parameters during the distance fits, the donor−acceptor distance distribution in the single strand was determined experimentally using trFRET (data not shown) and fixed during the evaluation of junction trFRET data. Likewise, the fraction of dissociated ribozyme at the respective temperature was extracted from the UV melting curves (Figure 2D) and also held constant in the fits. Only the fractions of docked and undocked ribozyme complexes, as well as their distance distributions, were adjusted. All fits converged to $\chi^2 < 1.2$. An example of such a three-species fit (Figure 3) illustrates the quality of the evaluation.

The docking equilibrium for the 2WJ, 3WJ, and 4WJ ribozymes was studied with trFRET between 4 and 75 °C.

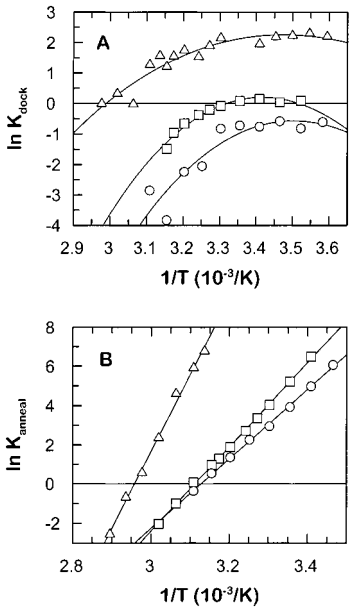

FIGURE 4: van't Hoff plots for the docking and annealing of 2WJ, 3WJ, and 4WJ ribozymes. (A) van't Hoff plot for docking of the different ribozymes: 2WJ (○), 3WJ (□), and 4WJ (△). Fitting a generalized van't Hoff model gives $\Delta C_p°$ values of −3.6 (2WJ), −3.9 (3WJ), and −1.7 kJ mol^{-1} K^{-1} (4WJ). The T_H and T_S values are 285 and 285 K (2WJ), 293 and 293 K (3WJ), and 288 and 291 K (4WJ). (B) van't Hoff plot for annealing: 2WJ (○), 3WJ (□), and 4WJ (△). The fits yield $\Delta H°_{anneal}$ values of −147 (2WJ), −178 (3WJ), and −326 kJ/mol (4WJ). The annealing entropies, $\Delta S°_{anneal}$, are −460, −555, and −965 J mol^{-1} K^{-1}, respectively.

From the fractions of docked, extended, and dissociated ribozymes, the equilibrium constants for the tertiary structure (K_{dock} = fraction docked/fraction extended) and the secondary structure transitions (K_{anneal} = fraction extended/fraction single strand) were calculated at all temperatures, and van't Hoff plots for the two steps were constructed (Figure 4). The van't Hoff plots for docking exhibit significant curvature for all three junction complexes, indicating that a change in heat capacity, $\Delta C_p°$, is associated with docking. The formation of secondary structure, in contrast, does not involve a change in heat capacity as indicated by the linear van't Hoff plots.

Global Fits. On the basis of the results from the separate van't Hoff plots, the temperature dependence of the population of the three species in equilibrium was globally analyzed in terms of a model assuming two consecutive structural changes as the ribozyme unfolds, i.e., a tertiary structure transition (undocking) that is associated with a change in heat capacity and a subsequent dissociation step that is characterized by $\Delta H°$ and $\Delta S°$ that are independent of temperature (Figure 5). For all three junction complexes, the fits describe the experimental data very well. The excellent fit for the dissociated ribozyme reflects the lack of noise in these values as they were extracted from the fits of the UV melting curves. The traces for all ribozyme constructs show that the undocked ribozyme is only to some extent populated in the tertiary structure transition region.

Table 2 summarizes the thermodynamic data for docking and annealing obtained from the global fits. For the 2WJ and 3WJ ribozymes, $\Delta H°_{anneal}$, $\Delta S°_{anneal}$, and $\Delta G°_{anneal}$ show excellent agreement with the apparent values obtained from the UV melting curves (Table 1), corroborating the fact that

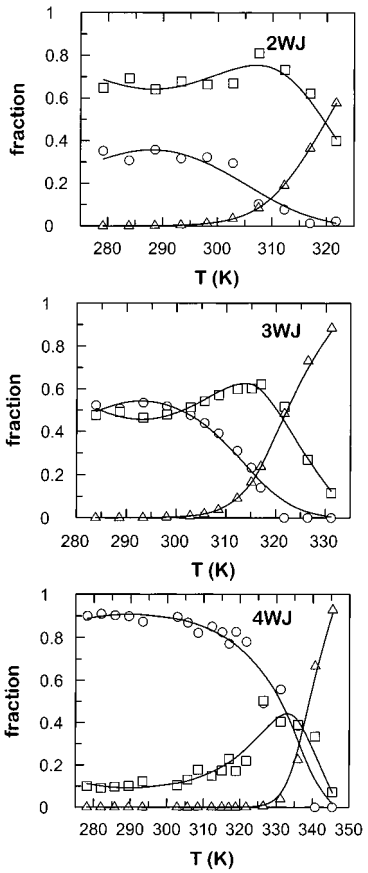

FIGURE 5: Global fits for docking and annealing thermodynamics of the hairpin ribozyme constructs. The fractions of docked (○), undocked (□), and dissociated (△) ribozyme species as determined from trFRET and UV melting data are shown as a function of temperature. The fraction of dissociated ribozyme was extracted from the UV melting curves (Figure 2D). The fractions of docked and extended ribozymes were determined from distance fits to trFRET data, including the dissociated ribozyme as a third species. The global fit to the data (solid lines) was performed assuming that the disruption of tertiary structure with a change in ΔC_p° precedes the secondary structure melting (no change in ΔC_p°) as deduced from the shape of the separate van't Hoff plots (Figure 4). The thermodynamic data derived from the fits are summarized in Table 2.

Table 2: Thermodynamics of Ribozyme Secondary and Tertiary Structure[a]

	2WJ	3WJ	4WJ
ΔC_p° (J mol^{-1} K^{-1})	−3903 (±1809)	−3980 (±1213)	−2132 (±877)
T_H (K)	288 (±1.2)	293 (±0.6)	290 (±3.1)
T_S (K)	287 (±1.2)	293 (±0.6)	293 (±2.6)
ΔH°_{dock} (kJ/mol)	−40.5 (±18.9)	−21.7 (±2.7)	−17.3 (±9.7)
ΔS°_{dock} (J mol^{-1} K^{-1})	−143 (±71)	−72 (±23)	−40 (±24)
ΔG°_{dock} (J/mol)	2117	−314	−5467
K_{dock}	2.4	1.1	9.1
ΔH°_{anneal} (kJ/mol)	−153 (±26)	−179 (±7)	−332 (±7)
ΔS°_{anneal} (J mol^{-1} K^{-1})	−479 (±82)	−555 (±22)	−982 (±21)
ΔG°_{anneal} (kJ/mol)	−10.5	−13.1	−39.1
K_{anneal}	69	197	7.1×10^6

[a] The global fits yield ΔC_p°, T_H, and T_S for docking as well as ΔH°_{anneal} and ΔS°_{anneal} together with their standard deviations. ΔH°_{dock}, ΔS°_{dock}, ΔG°_{dock}, K_{dock}, ΔG°_{anneal}, and K_{anneal} (all at 25 °C) and the standard deviations for ΔH°_{dock} and ΔS°_{dock} were calculated as described in Experimental Procedures.

the hyperchromicity reports solely on disruption of secondary structure and thus also reflects the isolated dissociation step. This behavior results from the considerable difference in the melting temperature T_m for the tertiary and secondary structures of the 2WJ and 3WJ ribozymes. For the 4WJ ribozyme, the apparent thermodynamic quantities derived from the UV melting profile reflect approximately the sum of the respective values for annealing and docking derived from the global analysis. The T_m values for the 4WJ ribozyme tertiary and secondary structure can be determined from the results of the global analysis to be 333 K (tertiary structure) and 338 K (secondary structure), respectively, indicating that in case of the 4WJ ribozyme, these transitions are thermodynamically coupled.

As deduced from the separate van't Hoff plots, the formation of tertiary structure is accompanied by a significant decrease in heat capacity. With values of −3.9 and −4.0 kJ mol^{-1} K^{-1}, ΔC_p° is almost the same for the 2WJ and 3WJ and smaller for the 4WJ (−2.1 kJ mol^{-1} K^{-1}). The calculated stabilities of the docked conformers agree with the experimental findings on the equilibrium distributions of docked and undocked conformers. Docking of the 2WJ complex is slightly endergonic; therefore, the undocked conformer is slightly favored at ambient temperature (25 °C). For the 4WJ, ΔG°_{dock} is negative and favors the docked conformer by a factor of 9. In the 3WJ, the docked and undocked conformers are equally stable.

When the ΔH°_{dock} values are compared, it becomes obvious that the differences in tertiary structure stabilities of the ribozyme junctions are not caused by the enthalpic term. In fact, ΔH°_{dock} is most favorable for the 2WJ and least favorable for the 4WJ. The entropic cost for docking, however, is highest for the 2WJ and overcompensates for ΔH°_{dock}, whereas in the 4WJ, ΔS°_{dock} is small. This indicates that the docked conformer of the 4WJ ribozyme is more stable because it is entropically less unfavored than the 2WJ and 3WJ ribozymes.

DISCUSSION

Method and Validity of the Approach. To learn about the thermodynamic factors that govern folding of RNA helical junctions, we have investigated the folding of the hairpin ribozyme containing different helical junctions. To extract thermodynamic parameters for the overlapping secondary and tertiary structure transitions, information from UV melting profiles (secondary structure) and trFRET (tertiary structure) were combined. trFRET has been successfully applied before to analyze equilibrium mixtures of nucleic acid conformational isomers (*1*, *15*−*17*). However, in these examples, only two conformers were present, whereas in this study, a third species had to be taken into account. Constraining the fractional population of this third species, the dissociated ribozyme, as well as the parameters describing its distance distribution to values determined in independent experiments reduced the degrees of freedom during the fit and afforded reliable results for the fractional populations and distance distributions of the docked and undocked ribozymes.

UV melting curves are an established means of gaining information about protein folding thermodynamics (*18*, *19*), and the same approach can be applied to nucleic acids (*20*−*22*). Absorbance melting curves have a high sensitivity and provide accurate values for ΔH and ΔS with standard errors of typically 5−8%. Due to compensating errors of ΔH and ΔS, ΔG is usually precisely determined. Alternatively,

enthalpies can be measured directly in a calorimeter to yield thermodynamic parameters that are model-independent. Substantially more material is required, however. Several comparative studies of ribonucleic acid secondary structure stability using absorbance melting curves and calorimetry in parallel have shown that analysis of UV melting curves yields valid thermodynamic information (*23*−*26*). Even complex unfolding events comprising multiple transitions can be described well assuming a sequence of partial unfolding events. It is not trivial, however, to assign a particular structural change to each observed transition. With the hairpin ribozyme, a single transition was observed, showing that all helices melt cooperatively. The interpretation of the ribozyme melting curves thus was unambiguous.

The Secondary and Tertiary Structure Transitions of the Hairpin Ribozyme Overlap and Are Differentially Sensitive toward Mg^{2+}. Although helical junctions are important motifs that are ubiquitous in RNA structures, no thermodynamic data on junction folding are available. In the hairpin ribozyme, the nature of the helical junctions joining the two loops that comprise the catalytically important positions determines the stability of the overall tertiary structure (*1*). Therefore, the hairpin ribozyme is a well-suited model system for studying the influence of helical junctions on folding. However, while the 2WJ and 3WJ ribozyme tertiary structures are disrupted at 40−50 °C in the presence of 12 mM Mg^{2+}, the tertiary structure of the 4WJ ribozyme is stable even at 60 °C under these conditions (*1*). Lowering the Mg^{2+} concentration to 1 mM, which represents physiological conditions, significantly destabilizes the tertiary structure for all three junctions and shifts the structural transition to lower temperatures that are spectroscopically accessible.

Tertiary structures have been reported to be sensitive to the concentration of Mg^{2+} ions, presumably because they form compact structures with high negative charge density that require stabilization by screening ions (*23*, *27*, *28*), whereas RNA secondary structures are not affected or only slightly affected by Mg^{2+} concentration. Consistent with this, UV melting curves of the 2WJ ribozyme at 1, 5, and 12 mM Mg^{2+} showed that the stability of the hairpin ribozyme secondary structure is sensitive toward the Mg^{2+} concentration to some extent (shift in T_m from 48 to 52 °C, data not shown), while the extent of 2WJ docking is increased from 10 to 70% in the same range of Mg^{2+} concentrations (*1*). Despite this rather selective stabilizing effect of Mg^{2+} ions on tertiary structure, however, the secondary and tertiary structure transitions still overlap at 1 mM Mg^{2+}. The same behavior has been observed for tRNA (*29*) and an RNA pseudoknot (*23*). In contrast, in the *Tetrahymena* group I intron ribozyme (*30*), certain tRNAs (*28*, *31*), and rRNA fragments (*32*), the tertiary structure unfolds first at lower temperatures and is extremely sensitive toward the Mg^{2+} concentration, while the secondary structure melts at a higher temperature. From these results, a picture emerged where the formation of tertiary structure can be envisaged as a separate thermodynamic and structural process of adding interactions to the lowest-free energy secondary structure (*23*).

This strict separation of secondary and tertiary structure transitions seems not to be applicable to the hairpin ribozyme. Even though the tertiary structures contribute not more than 12% to the overall stability at ambient temperature (Table 2), only in the context of a 4WJ ribozyme is the undocked species populated to a significant extent before the secondary structure unfolds at higher temperatures. The fraction of undocked 2WJ and 3WJ ribozymes does not increase significantly at higher temperatures, indicating that once the tertiary interactions are overcome, the junctions' secondary structure is only marginally stable and the molecules unfold completely. In tRNA, tertiary structure becomes more stable than secondary structure under certain salt conditions (*24*). Studies on a mRNA pseudoknot even suggested that the formation of tertiary structure may preferentially stabilize a secondary structure that is not the most stable on its own (*23*). This is also the case for a 3WJ in the *Tetrahymena* ribozyme that adopts a base-paired secondary structure in the absence of Mg^{2+} that corresponds to the lowest free energy minimum, but rearranges upon Mg^{2+}-induced formation of tertiary structure (*33*, *34*).

Altogether, these results support the hypothesis that RNA folding is not necessarily a hierarchical process but that secondary and tertiary structure transitions may be coupled. In this respect, the situation in RNA folding appears to be quite similar to folding of proteins where some proteins fold in a hierarchical manner with molten globule intermediates that exhibit secondary structure but lack long-range tertiary contacts, while in others, tertiary interactions are formed before the formation of secondary structure has been completed. Also, the overall stabilities of the helical junction ribozymes are similar to the stabilization energies found in proteins.

Role of Entropy in the Thermodynamic Stability of Secondary and Tertiary Structures. It has been observed in earlier studies that overall melting enthalpies of RNA do not significantly depend on temperature (*35*). This is true for the 2WJ, 3WJ, and 4WJ ribozymes, as can be deduced from the linear van't Hoff plots. However, substantial ΔC_p values for RNA folding have been found in cases where significant tertiary structure was present (*23*). While secondary structure formation of the junction ribozymes does not involve a change in heat capacity, docking is associated with a negative $\Delta C_p°$, suggesting that folding into the more compact docked structure buries some hydrophobic surface. The $\Delta C_p°$ values for the 2WJ and 3WJ are virtually identical (−3.9 and −4.0 kJ mol^{-1} K^{-1}), whereas formation of the docked 4WJ ribozyme is characterized by a smaller $\Delta C_p°$ of −2.1 kJ mol^{-1} K^{-1}. The values compare reasonably well with a $\Delta C_p°$ of −6.6 kJ mol^{-1} K^{-1} that has been measured for a DNA 3WJ (*36*). The smaller $\Delta C_p°$ value for the 4WJ ribozyme might be due to the already more compact secondary structure. Generally, RNA four-way helical junctions fold by pairwise coaxial stacking of helices that either are perpendicular or form a distorted antiparallel structure (*37*, *38*). However, within the experimental error, the difference in $\Delta C_p°$ between the ribozymes might not be significant.

The $\Delta H°_{dock}$ values for the ribozymes are on the same order of magnitude as for the tertiary structures of a DNA 3WJ (*36*) and a RNA pseudoknot (*26*). Unexpectedly, docking enthalpies indicate more favorable interactions in the docked 2WJ ribozyme than in the 3WJ and 4WJ. When the experimental errors are considered, the differences in $\Delta H°$ may be less pronounced than the values indicate. However, in a flexible 2WJ, a more favorable orientation of hydrogen bonds that contribute more stabilizing energy than in a

conformationally restricted 4WJ could be envisaged. A recent study on the *Tetrahymena* ribozyme suggested that rigid secondary structure elements might provide precise positioning of groups interacting in tertiary structure and thus contribute to tertiary structure stabilization (*39*), while in the context of a more flexible structure, unfavorable interactions can be accommodated with a less pronounced effect on the overall stability. This supports the notion that in the 4WJ ribozyme, tertiary interactions may not lead to the same negative $\Delta H°_{dock}$ as in the 2WJ ribozyme because they are not precisely positioned and the restricted internal flexibility does not allow for local rearrangements to improve the relative orientations.

Despite the smaller docking enthalpy, the 4WJ ribozyme exhibits the most stable tertiary structure. The greater stability results from a lower entropic cost for docking than for the 2WJ and 3WJ ribozymes. Presumably, the 4WJ restricts the conformational flexibility of the undocked complex, thereby reducing the entropic cost of forming the docked structure. The 4WJ may also help to preorganize the two helix−loop−helix elements for docking. In contrast, with a less constrained 2WJ, the undocked complex is more flexible, and the entropic cost of docking is correspondingly higher. These results underscore the importance of entropic effects on tertiary structure formation in RNA. Considerable stabilization energy can be gained by minimizing unfavorable entropy changes during folding.

Although entropic effects are important in understanding the overall tertiary structure stability of the hairpin ribozyme, docking is not entropically driven at 25 °C, in contrast to an equivalent docking process in the *Tetrahymena* ribozyme (*40*). The entropy change for docking is negative in all junctions, but this is compensated to varying degrees by a favorable $\Delta H°_{dock}$ term. The negative $\Delta C_p°$ associated with docking of the hairpin ribozyme predicts cold denaturation, however, as has been observed for the *Tetrahymena* ribozyme as well as in proteins (*40*, *41*). $\Delta S°_{dock}$ becomes positive below 14 °C for the 2WJ ribozyme, and below 20 °C for the 3WJ and 4WJ ribozymes.

Implications for the Role of Junctions in RNA Folding. The strong enthalpy−entropy compensation leads to a small negative $\Delta G°_{dock}$ for the 3WJ ribozyme and an even slightly positive $\Delta G°_{dock}$ for the 2WJ. This may be an important feature of these junctions as the conformational changes are readily reversible. The 4WJ, in contrast, seems to provide a scaffold for a stable tertiary structure that is crucial for ribozyme activity.

Helical branchpoints are ubiquitous elements in large RNAs and serve as hinge regions for conformational transitions. A conformational change in the central 3WJ of the 16S ribosomal RNA that brings two helical arms into proximity requires Mg^{2+} ions or binding of the ribosomal protein S15 (*42*). Likewise, the formation of the hammerhead ribozyme wishbone from the unfolded 3WJ requires a bulge in the interhelical junction as well as Mg^{2+} ions (*43*, *44*). In bacteriophage RNAs, conformational transitions within 3WJs and 4WJs have been sugggested to be important in the regulation of translation of the viral RNA (*45*). In the U1 snRNA, a prominent 4WJ appears to organize the structure of the entire RNA molecule (*46*). In contrast to 3WJs, RNA 4WJs form one predominant stacking conformer by pairwise coaxial stacking of the helices (*37*, *38*). Thus, in general, 4WJs appear to be important as structural scaffolds, whereas 2WJs and 3WJs confer flexibility on the tertiary structure and provide a potential requirement for regulatory ligands on the tertiary structure transition.

Like proteins, RNA tertiary structure seems to be stabilized by a small excess of favorable over unfavorable interactions. In the ribose zipper in the *Tetrahymena* ribozyme, a reciprocal pair of hydrogen bonds contributes ∼4.2 kJ/mol to the tertiary structure stability (*47*). This energy would be almost sufficient to explain the free energy stabilizing the 4WJ hairpin ribozyme. Interestingly, a similar ribose zipper has been proposed for the hairpin ribozyme (*48*, *49*). Favorable interactions are not the only determinants of tertiary structure, however. Our comparison of the helical junction ribozymes shows that different entropic costs can have a large impact on the stability of the final fold. In large RNA molecules, helical junctions may contain bulges of different sizes that further influence the global fold. While stacking of helices in 3WJs is favored by bulges, in the context of a 4WJ the flexibility induced by a bulge may render docking less efficient (*1*, *50*, *51*). Thus, RNAs can employ a wealth of different small adjustments in sequence to fine-tune their tertiary structure stability. A complex interplay between various structural elements allows for realization of any structural arrangement required for stability and biological function. This resembles the situation in proteins where subtle differences in sequence and tertiary structure can lead to a substantial stabilization of a thermophilic homologue compared to its mesophilic counterpart. It remains to be seen whether RNAs from thermophilic organisms employ the same strategy as proteins. Entropy−enthalpy compensations that lead to a marginal stabilization and ensure reversiblity as a prerequisite for flexibility and activity seem to play an important role in both proteins and RNAs. RNA helical junctions are a simple yet versatile structural element for implementing different requirements in RNA structure and biological function.

ACKNOWLEDGMENT

We thank Nils Walter for providing the double-labeled RNA strand, for the initial experiment on the temperature dependence of docking that motivated this study, and for helpful suggestions. We also thank John Burke and Ken Hampel for generously providing RNA strands, Markus Rudolph for helpful comments on the manuscript, and Michael Bailey and Markus Rudolph for stimulating discussions.

REFERENCES

1. Walter, N. G., Burke, J. M., and Millar, D. P. (1999) *Nat. Struct. Biol. 6*, 544−549.
2. Brion, P., and Westhof, E. (1997) *Annu. Rev. Biophys. Biomol. Struct. 26*, 113−137.
3. Pan, J., Thirumalai, D., and Woodson, S. A. (1997) *J. Mol. Biol. 273*, 7−13.
4. Rook, M. S., Treiber, D. K., and Williamson, J. R. (1998) *J. Mol. Biol. 281*, 609−620.
5. Chen, S.-J., and Dill, K. A. (2000) *Proc. Natl. Acad. Sci. U.S.A. 97*, 646−651.
6. Hampel, A., Tritz, R., Hicks, M., and Cruz, P. (1990) *Nucleic Acids Res. 18*, 299−304.
7. Chowrira, B. H., and Burke, J. M. (1991) *Biochemistry 30*, 8518−8522.

8. Berzal-Harranz, A., Joseph, S., Chowrira, B. M., Butcher, S. E., and Burke, J. M. (1993) *EMBO J. 12*, 2567−2573.
9. Murchie, A. I. H., Thomson, J. B., Walter, F., and Lilley, D. M. J. (1998) *Mol. Cell 1*, 873−881.
10. Walter, F., Murchie, A. I. H., and Lilley, D. M. J. (1998) *Biochemistry 37*, 17629−17636.
11. Walter, F., Murchie, A. I. H., Thomson, J. B., and Lilley, D. M. J. (1998) *Biochemistry 37*, 14195−14203.
12. Walter, N. G., Hampel, K. J., Brown, K. M., and Burke, J. M. (1998) *EMBO J. 17*, 2378−2391.
13. Thomson, J. B., and Lilley, D. M. J. (1999) *RNA 5*, 180−187.
14. Hampel, A., and Tritz, R. (1989) *Biochemistry 28*, 4929−4933.
15. Eis, P. S., and Millar, D. P. (1993) *Biochemistry 32*, 13852−13860.
16. Hochstrasser, R. A., Chen, S.-M., and Millar, D. P. (1992) *Biophys. Chem. 45*, 133−141.
17. Miick, S. M., Fee, R. S., Millar, D. P., and Chazin, W. J. (1997) *Proc. Natl. Acad. Sci. U.S.A. 94*, 9080−9084.
18. Schmid, F. X. (1989) in *Protein Structure: A Practical Approach* (Creighton, T. E., Ed.) pp 261−298, Oxford University Press, New York.
19. Pace, C. N. (1975) *CRC Crit. Rev. Biochem. 3*, 1−43.
20. Breslauer, K. J. (1987) *Methods Enzymol. 259*, 221−242.
21. Puglisi, J. D., and Tinoco, I. (1989) *Methods Enzymol. 180*, 304−325.
22. Draper, D. E., and Gluick, T. C. (1995) *Methods Enzymol. 259*, 281−305.
23. Gluick, T. C., and Draper, D. E. (1994) *J. Mol. Biol. 241*, 246−262.
24. Laing, L. G., and Draper, D. E. (1994) *J. Mol. Biol. 237*, 560−576.
25. Gluick, T. C., Wills, N. M., Gesteland, R. F., and Draper, D. E. (1997) *Biochemistry 36*, 16173−16186.
26. Nixon, P. L., and Giedroc, D. P. (2000) *J. Mol. Biol. 296*, 659−671.
27. Cole, P. E, Yang, S. K., and Crothers, D. M. (1972) *Biochemistry 11*, 4358−4368.
28. Stein, A., and Crothers, D. M. (1976) *Biochemistry 15*, 160−167.
29. Johnston, P. D., and Redfield, A. G. (1981) *Biochemistry 20*, 3996−4006.
30. Banerjee, A. R., Jaeger, J. A., and Turner, D. H. (1993) *Biochemistry 32*, 153−163.
31. Crothers, D. M., Cole, P. E., Hilbers, C. W., and Shulman, R. G. (1974) *J. Mol. Biol. 87*, 63−88.
32. Laing, L. G., Gluick, T. C., and Draper, D. E. (1994) *J. Mol. Biol. 237*, 577−587.
33. Wu, M., and Tinoco, I. (1998) *Proc. Natl. Acad. Sci. U.S.A. 95*, 11555−11560.
34. Thirumalai, D. (1998) *Proc. Natl. Acad. Sci. U.S.A. 95*, 11506−11508.
35. Privalov, P. L., and Filiminov, V. V. (1978) *J. Mol. Biol. 122*, 447−464.
36. Ladbury, J. E., Sturtevant, J. M., and Leontis, N. B. (1994) *Biochemistry 33*, 6828−6833.
37. Duckett, D. R., Murchie, A. I. H., and Lilley, D. M. J. (1995) *Cell 83*, 1027−1036.
38. Walter, F., Murchie, A. I. H., Duckett, D. R., and Lilley, D. M. J. (1998) *RNA 4*, 719−728.
39. Narlikar, G. J., Bartley, L. E., and Herschlag, D. (2000) *Biochemistry 39*, 6183−6189.
40. Narlikar, G. J., and Herschlag, D. (1996) *Nat. Struct. Biol. 3*, 701−710.
41. Privalov, P. L. (1990) *Crit. Rev. Biochem. Mol. Biol. 25*, 281−305.
42. Batey, R. T., and Williamson, J. R. (1998) *RNA 4*, 984−997.
43. Tuschl, T., Gohlke, C., Jovin, T. M., Westhof, E., and Eckstein, F. (1994) *Science 266*, 785−789.
44. Wedekind, J. E., and McKay, D. B. (1998) *Annu. Rev. Biophys. Biomol. Struct. 27*, 475−502.
45. Poot, R. A., Tsareva, N. V., Boni, I. V., and van Duin, J. (1997) *Proc. Natl. Acad. Sci. U.S.A. 94*, 10110−10115.
46. Branlant, C., Krol, A., and Ebel, J. P. (1981) *Nucleic Acids Res. 9*, 841−858.
47. Silverman, S. K., and Cech, T. R. (1999) *Biochemistry 38*, 8691−8702.
48. Earnshaw, D. J., Masquida, B., Muller, S., Sigurdson, S. T., Eckstein, F., Westhof, E., and Gait, M. J. (1997) *J. Mol. Biol. 274*, 197−212.
49. Ryder, S. P., and Strobel, S. A. (1999) *J. Mol. Biol. 291*, 295−311.
50. Gohlke, C., Murchie, A. I. H., Lilley, D. M. J., and Clegg, R. M. (1994) *Proc. Natl. Acad. Sci. U.S.A. 91*, 11660−11664.
51. Zacharias, M., and Hagerman, P. J. (1995) *J. Mol. Biol. 247*, 486−500.

BI0014103